

Comprehensive electro-thermal model of 26650 lithium battery for discharge cycle under parametric and temperature variations



C.S. Chin^{a,b,*}, Z. Gao^c, C.Z. Zhang^b

^a Faculty of Science, Agriculture, and Engineering, Newcastle University in Singapore, 599493 Singapore

^b School of Automotive Engineering; The State Key Laboratory of Mechanical Transmissions, Chongqing Automotive Collaborative Innovation Center, Chongqing University, Chongqing, 400044, China

^c School of Engineering, Clean Energy Research Centre, Temasek Polytechnic, 21 Tampines Avenue 1, 529757, Singapore

ARTICLE INFO

Keywords:
26650 LiFePO₄ battery cell
Electro-thermal model
Ambient temperature
Core temperature
Surface temperature
Battery stack

ABSTRACT

Ambient temperature affects the electro-thermal performance of lithium iron phosphate (LiFePO₄) batteries in electric vehicles. This paper proposes a combined electro-thermal state-space model for estimating the surface and core temperature of the battery cell and stack. A detailed experimental setup is used to determine the internal resistance and resistor-capacitor (RC) model of the electrical battery cell model and relationships between state-of-charge (SOC), open-circuit voltage and terminal voltage values at different ambient temperatures. The coupling between the electrical and thermal model provides estimation of voltage, core and surface temperatures under thermal uncertainties using measurable voltage, current and ambient temperature. The open-circuit voltage remains quite independent with ambient temperature at SOC value between 0.3 to 0.95 with a higher variation at 5 °C and 15 °C. The thermal parameters are identified as 2.23 k/W, 71.5 J/K and 4.35 k/W, respectively. The difference between the surface and ambient temperature is around 3.6 K as compared to core and surface temperature of around 2 K. The mean square error of the surface temperature between measurement and simulation of the battery stack is around 3 °C.

1. Introduction

Lithium iron phosphate (LiFePO₄) batteries have become popular for renewable energy storage devices, electric vehicles [1–3] and smart grids [4–6]. However, the batteries are quite vulnerable to temperature variation and unforeseen operating conditions such as overly charged or discharged affecting its performance and lifespan. Therefore, it is essential to obtain reasonably accurate cell model for the subsequent state of charge (SOC) estimation as it depends not only on the efficiency, self-discharging rate and load current, the temperature of the cells has to be considered. The internal or core temperature [7] of the battery cell can differ from the surface temperature under certain operating conditions. A set of model parameters obtained at a certain temperature is not robust for real-time operation. Therefore, using a thermal model to predict the core temperature under different operating conditions can enhance the overall model in the battery management system (BMS). Many papers involved the thermal modeling of the battery cell. The thermal model is combined with an electrical and chemical model forming an electrochemical thermal model [8] to determine the temperature response. In this paper, the electrochemical

thermal model will not be discussed. Instead, the thermal model followed by electro-thermal model will be discussed.

A Sony US18650 lithium-ion cell under different conditions such as cooling rate [9] was studied. The studies are useful if the external cooling device is used to prevent excessive heat dissipation involving different types of cell such as LiFePO₄ cell (model 18650) [10] and the FreedomCAR cell model [11]. Three-dimensional (3D) thermal models on large format cells (model D50H90) were used to provide insight into the temperature distributions under a condition such as abuse [12]. However, it did not predict the temperature of the cells under normal operating conditions where the batteries will be operating.

In addition, a low computational microcontroller used in most BMS does not allow the computationally demanding task of computing the 3D thermal model. As a result, a regression-based model [13] was proposed to estimate the cell temperatures at different SOC values and current levels. However, the model depends on the chemical properties of the LiFePO₄ cell (model 26650) that is quite complex to determine accurately. The dependence of the thermal properties [14] (for Sony US18650 lithium-ion cell) such as heat capacity and thermal conductivity on open-circuit voltage was also examined. However, the

* Corresponding author.

E-mail address: cheng.chin@ncl.ac.uk (C.S. Chin).

Nomenclature			
R	radius of battery cell m		
L	length of battery cell m		
h	convection coefficient $\text{W}/\text{m}^2\text{K}$		
c_p	specific heat capacity $\text{J kg}^{-1} \text{K}^{-1}$		
k	thermal conductivity W/mK		
T_a	ambient temperature K		
U_t	terminal voltage V		
U_1	voltage cross resistor-capacitor branch V		
I	load current A		
U_{oc}	open-circuit voltage V		
R_o	internal resistance Ω		
R_1	resistance in resistor-capacitor branch Ω		
C_1	capacitance in resistor-capacitor branch F		
K_0, K_1, K_2, K_3	constants used in open-circuit voltage - battery capacity Ah		
$f(\cdot)$	nonlinear function used in derivative of terminal voltage - convection resistance Ω		
R_s	conduction resistance Ω		
C_c	heat capacity of core $\text{J kg}^{-1} \text{K}^{-1}$		
C_s	heat capacity of surface $\text{J kg}^{-1} \text{K}^{-1}$		
Q	heat generation W		
R_d	lumped resistance Ω		
t	time s		
\mathbf{x}^i	state vector for i^{th} battery cell -		
\mathbf{y}^i	output vector for i^{th} battery cell -		
\mathbf{A}^i	system matrix for i^{th} battery cell -		
\mathbf{B}^i	input matrix for i^{th} battery cell -		
\mathbf{C}^i	output matrix for i^{th} battery cell -		
n	number of battery cells -		
R_1/R_2	radius ratio of battery cell -		
$T_{s,i}$	Surface temperature of i^{th} battery cell K		
ΔK	temperature gain factor K		
ΔU_0	instantaneous jump in voltage V		
R_{0,T_a}	R_0 at different ambient temperatures and state-of-charge value Ω		
m	number of samples for R_0 at different ambient temperatures -		
a, b	constants -		
t_{RC}	time interval at voltage transient during relaxation s		
J	cost function to minimize the voltage least square error V		
$U_{1,data}(z)$	measured relaxation voltage data for z time instant V		
$W(s)$	parametric observation in s-domain -		
\hat{R}_u	parameter estimates of $R_u \Omega$		
\hat{R}_c	parameter estimates of $R_c \Omega$		
\hat{C}_c	parameter estimates of $C_c \text{ J kg}^{-1} \text{K}^{-1}$		
$R_{0,5^\circ\text{C}}$	internal resistance at 5 °C Ω		
$R_{0,15^\circ\text{C}}$	internal resistance at 15 °C Ω		
$R_{0,25^\circ\text{C}}$	internal resistance at 25 °C Ω		
		$R_{0,35^\circ\text{C}}$	internal resistance at 35 °C Ω
		$R_{0,45^\circ\text{C}}$	internal resistance at 45 °C Ω
		t_d	discharge time s
		Q_d	static capacity Ah
		<i>Greek letters</i>	
		ρ	density of battery cell kg m^{-3}
		Δ	change -
		Φ	parameters used in model parameterization for thermal -
		θ	regressor used in model parameterization for thermal -
		δ, μ, σ	physical parameters used in model parameterization for thermal -
		$\hat{\delta}, \hat{\mu}, \hat{\sigma}$	estimated physical parameters used in model parameterization for thermal -
		$\hat{\theta}$	least square estimation
		<i>Subscripts and superscripts</i>	
		a	ambient temperature
		t	terminal
		0	initial/instantaneous
		c	core
		s	surface
		RC	resistor-capacitor branch
		C	conduction heat transfer
		h	convective heat transfer
		d	lumped
		dis	discharge
		<i>Abbreviations</i>	
		SOC	state-of-charge
		LiFePO4	lithium iron phosphate
		BMS	battery management system
		RC	single resistor and capacitor
		2RC	pair of resistor and capacitor
		3RC	three resistor and capacitor branches
		3D	three-dimensional
		2D	two-dimensional
		PDE	partial differential equation
		ECM	equivalent circuit model
		NMC	nickel-manganese-cobalt
		LTO	lithium titanate
		Ah	ampere hour
		OCV	open-circuit voltage
		RMSE	root mean square error
		MSE	mean square error
		DC	direct-current
		DAQ	data acquisition

model parameters obtained may not be robust for actual operation.

Hence, a simple thermal model [15] was developed to examine the thermal behavior of a battery stack (prismatic lithium-ion cells) using different simplification strategies for conductive, convective, and radiative heat transfer equations. The results could estimate the thermal behavior of the battery pack. However, the applications on cylindrical battery cells cannot be applied directly as the mode of heat transfer due to the cells' arrangement was different. The heat generated during rapid charge and discharge cycles [16] of Sony US18650 lithium-ion battery cell at different current levels was also studied. The thermal behavior such as the core and surface temperature of the cell showed a small difference of 0.2 °C to 3 °C using one-dimensional (1D) thermal conductive and convective heat transfer.

A thermal model in state-space equations was used to estimate the core temperature [17] of the LiFePO₄ battery cell (model 26650) via an online parameter identification approach and the surface temperature measurement. However, the electrical and thermal behavior under varying ambient temperatures and the impacts of uncertainties in the thermal parameters of the battery stack are not examined. Another thermal model using reduced-order state-space equations [18] via a polynomial approximation of the temperature in LiFePO₄ cell (model 18650) was examined. A dual Kalman filter was used to estimate the battery core temperature and convection coefficient. The results showed that the model could give an accurate prediction of the core temperature under uncertain cooling conditions. However, the electro-thermal behavior and the influence of ambient temperatures and

uncertainties of the thermal parameters of the battery stack are not studied. Another thermal model for a cylindrical battery based on the finite-element method [19] was developed. The paper emphasized on analyzing the temperature distributions of the cell at different conditions but lack of insight on how to use the finite-element model in BMS. Additionally, 1D thermal model [20] for cylindrical battery cells using a partial differential equation (PDE) observer-based technique was used. The PDE is quite complex to implement in actual BMS due to the high computational resource.

The same problem can be found in the model-free approach such as the spatial-temporal learning model [21] designed by the evolutionary algorithm to predict the thermal distribution. The computational resource was quite intensive to compute the detailed thermal distribution of the entire battery cell. It is not realistic to implement as both core and surface temperature are required. The transient and electrothermal finite element analysis [22] of a Lithium Cobalt Oxide(LiCoO₂) battery at various discharge rates was studied. The parametrization of the results into an electro-thermal model for actual implementation is not explicit.

Instead of using the thermal model, the electrical model of the cell to determine the terminal, open-circuit voltage and the SOC at different thermal conditions are included. A lumped-parameter electrical model approach [23,24] such as an equivalent circuit model of the LiFePO₄/graphite battery using the resistor and capacitor (RC) pairs was used due to its low complexity and simplicity for implementation. Combined with the two-state thermal model coupled via temperature dependence of the multiple-RC circuits and heat generation, the electro-thermal model could be obtained. However, the electrical circuit uses multiple RC pairs [23,24–26] that can increase the complexity of the electrical model as more parameters were identified. It was shown that a single RC pair [27,28] could be sufficient to model the terminal voltage of the battery cell. Alternatively, 2D-thermal and 2-RC electrical model [29] was used to estimate the voltage behavior and thermal distribution under dynamic and static load profiles of the Li-ion pouch cells. As battery consists of more than a cell, the study of the battery stack is required.

A fully coupled electro(2RC)-thermal model [24] was modeled as a linear-time-varying model with the unmeasurable battery internal states such as the SOC and core temperature of the LiFePO₄ cylindrical cells (model 26650). But the works were on control the time and core temperature increase instead of the thermal parameterization. Further research was performed using electro (2RC)-thermal behavior [30,31] of a lithium iron magnesium phosphate and LiFePO₄ cylindrical cells (model 18650 and 38120) on an electric vehicle under different drive tests. But the thermal model used the core temperature of the cells instead of both the core and surface temperature. An electro (2RC)-thermal model [32] of LiFePO₄ cylindrical cells (model 26650) based on the ECM was also examined. The parameterization of both the electrical and thermal model at different ambient temperatures was not studied.

In summary, the electrical model under varying ambient temperature and thermal model parameterization under model uncertainties for battery cell and stack using LiFePO₄ (model 26650) are marginally discussed. In addition, the electro-thermal model is likely to have higher precision [33–37] in practices due to its simplicity in the parameter identification. As a result, an electro (1RC)-thermal based model of LiFePO₄ cylindrical cell (model 26650) with consideration of the surface, core and ambient temperature variation are required. In summary, the contributions of this paper are as follows.

- As a contrast to works done in the estimation of the electro-thermal parameter [17,18,23], the proposed approach provides a detailed electrical circuit modeling and measurement under varying ambient temperature (instead of fixed ambient temperature) condition.
- The electrical model is coupled with the dual-state thermal model (to estimate both the core and surface temperature) for both battery

cells and stack under the thermal model uncertainties is proposed.

- The combined electro-thermal state-space model for estimating the surface and core temperature of 12-cell arranged in series (assuming constant heat generation) is derived.
- The coupling between the electrical and thermal stack model that can estimate the voltages, SOCs, surface and core temperatures under the thermal uncertainties using the measurable input current, voltage and ambient temperatures in both the battery cell and stack is proposed.
- All electrical (under varying ambient temperatures) and thermal parameters for LiFePO₄ cylindrical cells (model 26650) used are provided in a single paper.

The paper is organized as follows: The nonlinear electro-thermal model is derived in Section 2. Section 3 performs the parameterized electrical and thermal model. Section 4 presents the experiments and validation of the electro-thermal model. The results of the sensitivity tests are shown in this section. Section 5 concludes the paper.

2. Nonlinear electro-thermal battery cell and stack model

A lithium iron phosphate battery (LiFePO₄) battery cell of type ANR26650M1-B manufactured by A123 will be used in this paper. The main specifications from datasheet and parameters [23,38,46] of the cell can be seen in Table 1.

A combined electro-thermal model is established for LiFePO₄ battery cell. The terminal voltage is modeled by an equivalent circuit model (ECM) and a dual state thermal model is used to determine the surface and core temperatures. The ECM depends on SOC, temperature and current direction. While the parameters of the thermal model are obtained through the least square method.

2.1. Electrical battery cell model

The electrical and thermal model of the battery cell can be seen in Fig. 1. The electrical resistance of different battery components is represented by R_o . The single RC branch consisting of R_1 and C_1 that describes the dynamic voltage performances and mass transport effects. The values are obtained by a common constant-current/constant-voltage (CCCV) test where the battery cell charger controls the level of

Table 1

Battery cell specifications and parameters of LiFePO₄ of type ANR26650M1-B.

Specifications	Values
Radius (R)	13 mm
Length (L)	65.15 mm
Weight (W)	76 g
Cell Capacity (nominal/minimum) (0.5 C Rate)	2.5 Ah /2.4Ah
Nominal Voltage	3.3 V
Recommended Standard Charge Method	2.5 A to 3.6 V CCCV for 1 h
Cycle Life at 20 A Discharge, 100% DOD	>1000 cycles
Maximum Continuous Discharge	50 A
Operating Temperature	-30 °C to 55 °C
Storage Temperature	-40 °C to 60 °C
Cathode (LiFePO ₄)	
- Density	2300 kg/m ³
- Specific heat	1300 J/kg °C
Anode (Graphite)	
- Density	1347 kg/m ³
- Specific heat	1437 J/kg °C
Electrolyte (organic solution)	
- Density	1223 kg/m ³
- Specific heat	1375 J/kg °C
Density, ρ	1824 kg/m ³ [38]
Convection coefficient, h	5 W/m ² K[18, 38, 46]
Specific heat coefficient, c_p	825 J/kgK[38]
Thermal conductivity, k	0.488 W/mK[38]
Ambient temperature, T_a	298 K [23]

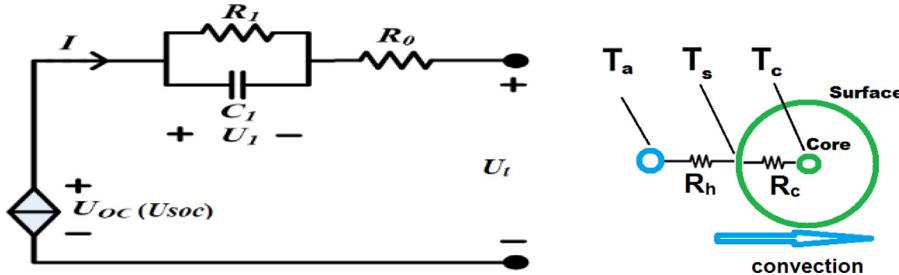


Fig. 1. Single RC cell model (left) and thermal model of LiFePO₄ cell (right).

current to a preset value until the cell obtains a terminal voltage (U_t) value. The open-circuit voltage(OCV) or U_{oc} is defined as the difference between two voltage terminals when disconnected from the circuit.

From the model in Fig. 1, the dynamic equations of the terminal voltage U_t can be derived.

$$\dot{U}_t = -\frac{1}{R_1 C_1} U_t + \frac{1}{C_1} I \quad (1)$$

$$U_t = U_{oc} - U_1 - R_0 I \quad (2)$$

where U_1 is the voltage cross the RC branch, U_t is the terminal voltage, I is the load current and the open-circuit voltage(OCV), U_{oc} can be defined as

$$U_{oc} = K_0 + K_1 SOC + K_2 In(SOC) + K_3 In(1 - SOC) \quad (3)$$

where K_0, K_1, K_2, K_3 are the constants used and its derivative is written as

$$\dot{U}_{oc} = K_1 S\dot{O}C + K_2 S\dot{O}C/SOC + K_3 S\dot{O}C/(SOC - 1) \quad (4)$$

where state-of-charge (SOC) can be estimated by the ampere hour (Ah) counting method using the current (I) and the nominal battery capacity in Ah (C_n)

$$S\dot{O}C = -\frac{1}{C_n} I \quad (5)$$

Note that coulombic efficiency is assumed to be 100% and the self-discharging rate is quite negligible.

By substituting U_1 , (2), (4) and (5) into the derivative of U_t (assuming constant I and R_0), it can be written as

$$\dot{U}_t = \dot{U}_{oc} - \dot{U}_1 \quad (6)$$

$$\begin{aligned} \dot{U}_t &= \frac{1}{R_1 C_1} [-U_t - R_0 I + (K_0 + K_1 SOC + K_2 In(SOC) + K_3 In(1 - SOC))] \\ &\quad - \frac{1}{C_1} I - \frac{1}{C_n} \left(K_1 + \frac{K_2}{SOC} - \frac{K_3}{1 - SOC} \right) I \end{aligned} \quad (7)$$

Rearranging (7) becomes

$$U_t = -\frac{1}{R_1 C_1} U_t - \left(\frac{R_0}{R_1 C_1} + \frac{1}{C_1} + \frac{K_1}{C_n} \right) I + \frac{K_0}{R_1 C_1} + \frac{K_1}{R_1 C_1} SOC + f(SOC, I) \quad (8)$$

where

$$f(SOC, I) = -\frac{1}{C_n} \left(\frac{K_2}{SOC} - \frac{K_3}{1 - SOC} \right) I + \frac{K_2}{R_1 C_1} InSOC + K_3 In(1 - SOC) \quad (9)$$

2.2. Thermal battery cell model

For the thermal model in Fig. 1, the temperature distribution in the longitudinal direction is more uniform than the radial direction due to the higher thermal conductivity [14,15,18]. The constant R_s and R_c are the convection resistance on the surface of the cell and heat conduction resistance in the core of the cell, respectively. T_a is the ambient

temperature, T_s is the surface temperature, C_c and C_s are the heat capacity of the core and surface, respectively. An uniform heat generation along the radial direction is assumed [22,39]. The thermal dynamics of a cylindrical battery cell in radial direction are modeled using the classical heat transfer approach by assuming no heat flux at the center and heat generation at the core. The dual-state approximation of the thermal model in radial direction [17,18,40] is defined as

$$\frac{dT_s}{dt} = \frac{T_a - T_s}{R_s C_s} - \frac{T_s - T_c}{R_c C_s} \quad (10a)$$

$$\frac{dT_c}{dt} = \frac{T_s - T_c}{R_c C_c} + \frac{Q}{C_c} \quad (10b)$$

The values of the parameters used in (10) will be estimated. The heat generation Q [17] is approximated as a concentrated source of Joule loss in the core determined by the product of the squared current and lumped resistance, R_d .

$$Q = I^2 R_d \quad (11)$$

2.3. Combined electro-thermal battery cell model

By considering both terminal voltage (U_t) and thermal model (T_s , T_c), a combined model in state-space form can be established. Defining $\mathbf{x}^i = [U_t \ T_s \ T_c]^T$ as the state vector and denoting the input vector as $\mathbf{u}^i = [I \ 1 \ SOC \ Q \ T_\infty]^T$ for i^{th} battery cell. The output $\mathbf{y}^i = [U_t \ T_s \ T_c]^T$ for i^{th} battery cell. The state and output equations of i^{th} battery cell are given by the following

$$\dot{\mathbf{x}}^i = \mathbf{A}^i \mathbf{x}^i + \mathbf{B}^i \mathbf{u}^i + f^i(SOC, I) \quad (12a)$$

$$\mathbf{y}^i = \mathbf{C}^i \mathbf{x}^i + \mathbf{D}^i \mathbf{u}^i, i = 1, 2, \dots n \quad (12b)$$

where $f^i(SOC, I)$ is the nonlinear function in (9) for i^{th} battery cell and the system matrix, \mathbf{A}^i with the following elements $A_{11}^i \in R$, $\mathbf{A}_{12}^i \in R^{1 \times 2}$, $\mathbf{A}_{21}^i \in R^{2 \times 1}$, $\mathbf{A}_{22}^i \in R^{2 \times 2}$ can be written as

$$\mathbf{A}^i = \begin{bmatrix} A_{11}^i & A_{12}^i \\ \mathbf{A}_{21}^i & \mathbf{A}_{22}^i \end{bmatrix} = \begin{bmatrix} -\frac{1}{R_1 C_1} & 0 & 0 \\ 0 & \left(\frac{1}{R_s C_s} + \frac{1}{R_c C_s} \right) & \frac{1}{R_c C_s} \\ 0 & \frac{1}{R_c C_c} & -\frac{1}{R_c C_c} \end{bmatrix} \quad (13b)$$

and input matrix

$$\mathbf{B}^i = \begin{bmatrix} \mathbf{B}_{11}^i & \mathbf{B}_{12}^i \\ \mathbf{B}_{21}^i & \mathbf{B}_{22}^i \end{bmatrix} = \begin{bmatrix} \frac{R_0}{R_1 C_1} + \frac{1}{C_1} + \frac{K_1}{C_n} & \frac{K_0}{R_1 C_1} & \frac{K_1}{R_1 C_1} & 0 & 0 \\ 0 & 0 & 0 & 0 & 1 \\ 0 & 0 & 0 & 0 & \frac{1}{C_c} \\ 0 & 0 & 0 & \frac{1}{C_c} & 0 \end{bmatrix} \quad (13b)$$

where $\mathbf{B}_{11}^i \in R^{1 \times 3}$, $\mathbf{B}_{12}^i \in R^{1 \times 2}$, $\mathbf{B}_{21}^i \in R^{2 \times 3}$, $\mathbf{B}_{22}^i \in R^{2 \times 2}$ and output matrix

$$\mathbf{C}^i = \begin{bmatrix} C_{11}^i & C_{12}^i \\ C_{21}^i & C_{22}^i \end{bmatrix} = \begin{bmatrix} 1 & 0 & 0 \\ 0 & 1 & 0 \\ 0 & 0 & 1 \end{bmatrix}; \mathbf{D}^i = 0 \quad (14)$$

where $C_{11}^i \in R$, $C_{12}^i \in R^{1 \times 2}$, $C_{21}^i \in R^{2 \times 1}$, $C_{22}^i \in R^{2 \times 2}$

Eq. (12) can be extended to battery stack of more than a cell. For

example, the matrix $\mathbf{A}^{1,\dots,n}$ with the following element can be formulated

$$\begin{aligned}\mathbf{A}^{1,\dots,n} &= \begin{pmatrix} \mathbf{A}^{i=1} & \dots & 0 \\ \vdots & \ddots & \vdots \\ 0 & \dots & \mathbf{A}^{i=n} \end{pmatrix} \mathbf{B}^{1,\dots,n} = \begin{pmatrix} \mathbf{B}^{i=1} & \dots & 0 \\ \vdots & \ddots & \vdots \\ 0 & \dots & \mathbf{B}^{i=n} \end{pmatrix} \mathbf{C}^{1,\dots,n} \\ &= \begin{pmatrix} \mathbf{C}^{i=1} & \dots & 0 \\ \vdots & \ddots & \vdots \\ 0 & \dots & \mathbf{C}^{i=n} \end{pmatrix}\end{aligned}\quad (15a)$$

$$\mathbf{x}^{1,\dots,n} = [\mathbf{x}^1 \dots \mathbf{x}^n]^T, \quad \mathbf{u}^{1,\dots,n} = [\mathbf{u}^1 \dots \mathbf{u}^n]^T, \quad (15b)$$

$$\mathbf{y}^{1,\dots,n} = [\mathbf{y}^1 \dots \mathbf{y}^n]^T \quad (15c)$$

where n is number of battery cells.

2.4. Electro-thermal battery stack model

Eqs. (12) to (15) assumed the heat generation, Q is similar for each cell (connected in series) as shown in Fig. 2. The core temperature of each cell is also assumed to be constant. The surface temperature of cell #1 is quite close to cell #2 as they are placed physically near to each other. However, the surface temperature of the cells in the stack can be different as heat is transferred from one cell to another.

The energy balance of a battery cell due to conduction and convection under constant heat generation, Q can be written as

$$Q = \frac{T_s - T_a}{1/(2\pi RL) + \ln(R_2/R_1)/2\pi K_c L} \quad (16)$$

Simplifying (16) gives

$$Q = \frac{2\pi L}{\frac{1}{R_h} + \frac{\ln(R_2/R_1)}{K_c}} (T_s - T_a) = \Delta K \cdot (T_s - T_a) \quad (17)$$

where the temperature gain factor is defined as

$$\Delta K = \frac{2\pi L}{\frac{1}{R_h} + \frac{\ln(R_2/R_1)}{K_c}} \quad (18)$$

where R is the radius of the cell and R_2/R_1 is the ratio of the radius, K_c is the conduction heat transfer coefficient, h is the convective heat transfer coefficient (see Table 1) and Q is the heat generation from the cell. The convective heat transfer coefficient, h can be estimated using a simplified relation for natural convection heat transfer coefficients for cylindrical geometry in air at atmospheric pressure for laminar flow conditions [45].

Hence, the surface temperature of the i^{th} cell can be sequentially computed as follows. It can be seen that the surface temperature is a summation of ambient temperature and multiple of $q/\Delta K$ of each cell that is arranged in series.

$$\begin{aligned}T_{s,1} &= Q/\Delta K + T_a \\ T_{s,2} &= Q/\Delta K + T_{s,1} = Q/\Delta K + Q/\Delta K + T_a \\ &\vdots \\ T_{s,n} &= Q/\Delta K + T_{s,n-1} = Q/\Delta K + Q/\Delta K + Q/\Delta K \dots + T_a\end{aligned}\quad (19)$$

where $i = 1, \dots, n$ is the i^{th} cell and n is the number of cells.

Eq. (19) can also be written in a compact form

$$T_{s,i} = \frac{Q}{\Delta K} \cdot i + T_a \quad (20)$$

Note that the T_a of the cell #1 will become the surface temperature of cell #2. As seen in Fig. 3, the electrical model computes U_b , U_{oc} and SOC of the battery using the load current and the electrical model parameters. The product of lumped resistance R_d and I determines the heat generation Q . The thermal model computes the surface and core temperature T_s and T_c , respectively. It also uses the ambient temperature T_a as an input to the thermal model. The surface temperature T_s will be used to determine the temperature-dependent parameters of the electrical model as it is difficult to measure the core temperature. The core temperature will be estimated by the least square approach as shown in Section 3.2. The electro-thermal model in Fig. 3 can estimate the terminal voltage, core and surface temperature of the battery cell.

3. Parameterization of electro-thermal cell model

The approach to parameterize the electro-thermal model is explained. The parameters in the electrical model are estimated based on a periodic pulse test conducted under a predetermined ambient temperature and SOC condition to determine the electrical model independently from the thermal model. Progressive testing under different ambient temperatures, SOCs and current directions (i.e. first charging and then followed by discharging) will be performed. The thermal model is then parameterized using the heat generated using the current, the voltage and the open-circuit voltage of the electrical model.

3.1. Cell model parameterization in electrical

The parameterization identifies the open-circuit voltage, internal resistance, capacitance and resistance of RC pair. As seen in Fig. 4, 1RC and 2RC electrical models are compared at ambient temperature. The root mean square error (RMSE) between the terminal voltage of 1RC and 2RC pair is around 3.277×10^{-4} V. It is shown that the difference is not very significant. Hence, the 1RC is used for the electrical model.

To obtain the electrical parameters, the battery cell is first fully charged to reach full SOC under the typical constant current-constant voltage (CC-CV) condition before the terminal voltage is relaxed for at least 45 min to reach equilibrium as seen in Fig. 4. The static capacity (in Ah) is then calculated as follows.

$$Q_d = \frac{1}{3600} \int_0^{t_d} I_d(\tau) d\tau \quad (21)$$

where I_d is the discharge current in ampere and t_d is the discharge time in second. The SOC is an expression of the present battery capacity as a percentage of maximum capacity. It is calculated using current integration to determine the change in battery capacity over time (i.e. the Ah counting method).

The cell is then discharged to SOC value of 0.9 with a current of 0.8C or 2A (where 1C is measured of the charge and discharge current with respect to its nominal capacity). The current is terminated to relax

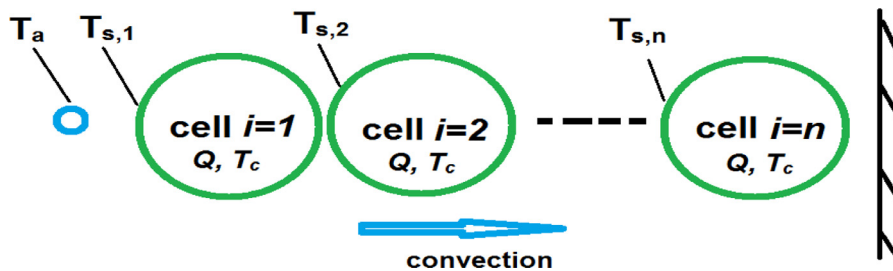


Fig. 2. Combined LiFePO4 cells in series to form battery stack .

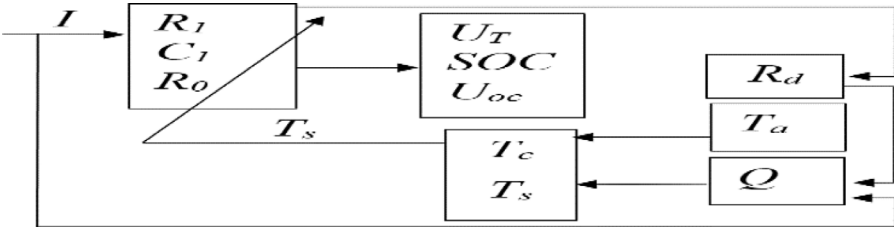


Fig. 3. Combined electro-thermal model of LiFePO₄ battery cell .

the battery for 45 min to reach equilibrium. The instantaneous jump in the voltage ΔU_0 after the injection of the current pulse allows the internal resistance, R_0 to be determined based on Ohm's law.

$$R_0 = \Delta U_0 / I \quad (22)$$

As there are multiple R_0 values determined from the pulse test, a mean value for representing R_0 at the different ambient temperatures and SOC values is given as

$$R_{0,T_a} = \sum_{i=1}^m R_{0,T_a,i} / m \quad (23)$$

where m is the number of samples and subscript T_a refers to R_0 at different ambient temperatures.

In addition, the value of R_{0,T_a} at different SOC range can be expressed as follows.

$$R_{0,T_a}(SOC) = a \cdot SOC + b \quad (24)$$

where a and b are the constant value.

On the other hand, the voltage transient during relaxation is used to

estimate the R_1 and C_1 parameter. The U_1 can be determined by solving (1) at each time interval, t_{RC} at voltage transient during relaxation.

$$U_1(t_{RC}) = R_1 I (1 - e^{-\frac{t_{RC}}{R_1 C_1}}) \quad (25)$$

where t is the pulse period prior to the relaxation.

The R_1 and C_1 parameter are then used to minimize the voltage least square error using the cost function, J as,

$$J = \min_{R_1, C_1} \sum_z [U_1(z) - U_{1,data}(z)]^2 \quad (26)$$

where $U_{1,data}(z)$ is the measured relaxation voltage data for z time instant and $U_1(z)$ is voltage evaluated via (1).

The steps to determine R_0 , R_1 and C_1 parameter via (22) to (26) can be repeated until the terminal voltage reached the final cut-off voltage of 2.5 V. During the test, the battery cell is inside the oven where the ambient temperature was controlled at a few set points, namely: 5 °C, 15 °C, 35 °C and 45 °C. The difference between the discharging and

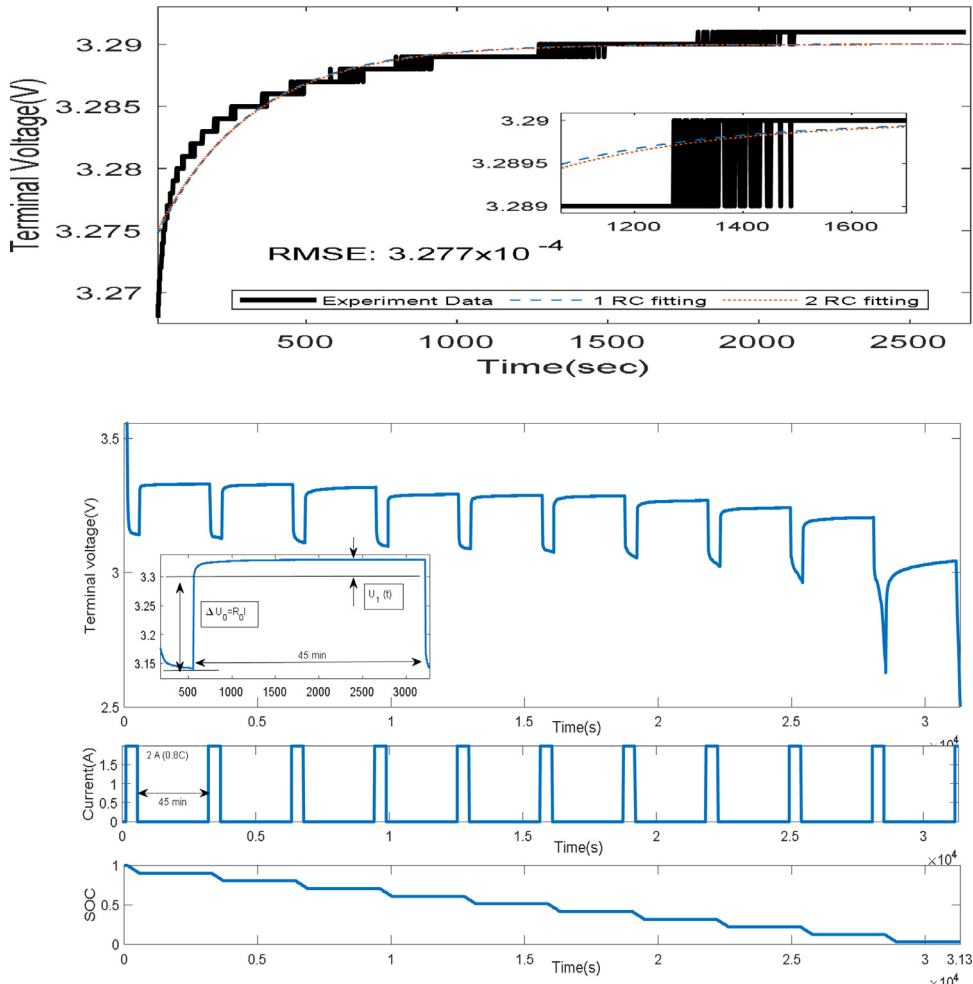


Fig. 4. Terminal voltage between 1RC and 2RC (top), terminal voltage, current input and SOC during pulse discharging test (bottom).

charging voltage due to hysteresis [41] can exist. To circumvent this, the average [18] value of the discharging and charging voltage is used as the OCV (refer to Fig. 5). The value of OCV (i.e. the terminal voltage at equilibrium occurred at around 45 min) was identified from the results of the pulse discharge test under 25 °C as shown in Fig. 4. The OCV for each SOC value (estimated by Ah counting method) can then be plotted as seen in Fig. 5.

3.2. Cell model parameterization in thermal

The parameters used in the thermal model consist of the convection resistance R_s , conduction resistance R_c , and heat capacities of the battery surface C_s and the core C_c are estimated by the approach [17,42,43]. As the measurement of the core temperature is difficult, the approach uses only the surface temperature T_s , the load current I and the ambient temperature T_a that can be easily measured.

The parametric model of thermal model in the s-domain is written as.

$$\mathbf{W}(s) = \boldsymbol{\theta}^T \Phi(s) \quad (27)$$

where Φ is the parameter, \mathbf{W} is the observation and $\boldsymbol{\theta}$ is the regressor including the measured parameters.

The thermal parametric model can be obtained via Laplace transformation of (10) and removing the T_c that is unmeasured by substituting with the measured signals.

$$s^2 T_s(s) = \frac{1}{R_c R_s C_c C_s} [T_a(s) - T_s(s)] + \frac{Q(s)}{R_c C_c C_s} - \left(\frac{1}{R_s C_s} + \frac{C_s + C_c}{R_c C_c C_s} \right) s T_s(s) \quad (28)$$

Expressing (28) into the form of (27), the following can be obtained.

$$\text{Regressors: } \Phi = [Q(s) \ T_a(s) - T_s(s) \ s T_s(s)]^T \quad (29a)$$

$$\text{Parameters: } \boldsymbol{\theta} = [\delta \ \sigma \ \mu]^T \quad (29b)$$

$$\text{Observations: } \mathbf{W} = s^2 T_s(s) \quad (29c)$$

The physical parameters can be defined as follows.

$$\sigma = 1/(R_c R_s C_c C_s) \quad (30a)$$

$$\delta = 1/(R_c C_c C_s) \quad (30b)$$

$$\mu = -(C_c R_s + C_c R_c + C_s R_s)/(R_c R_s C_c C_s) \quad (30c)$$

The least squares approach is applied to estimate Φ [42] as shown.

$$\hat{\boldsymbol{\theta}} = (\Phi^T \Phi)^{-1} \Phi^T \mathbf{W} \quad (31)$$

where $\hat{\boldsymbol{\theta}}$ an estimation of $\boldsymbol{\theta}$. The identification is conducted in time interval. Using (31), the parameters $[\delta \ \sigma \ \mu]^T$ can be estimated. Since three of the four terms can be determined using $[\delta \ \sigma \ \mu]^T$. The value C_s can be computed using the casing size and its specific heat capacity. The parameter estimates of R_s , R_c and C_c can be determined using the following relationships.

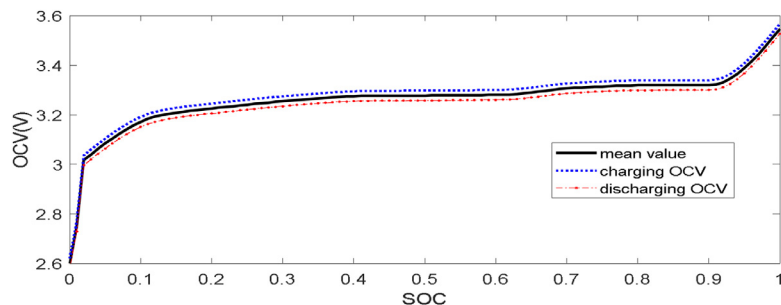


Fig. 5. Average OCV vs SOC for charging and discharging.

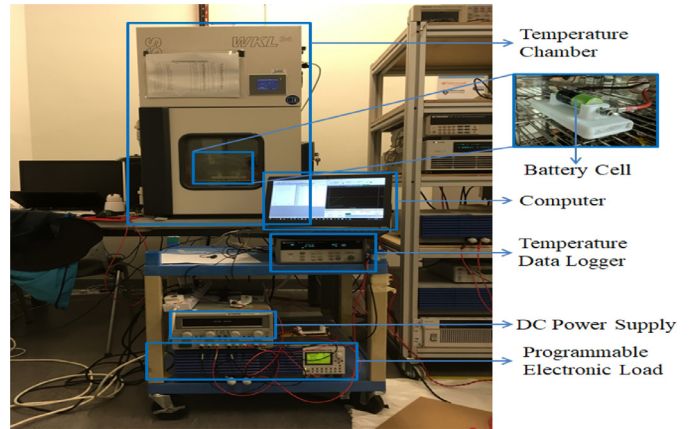


Fig. 6. Actual experiment setup for electrical model parameterization of ANR26650M1-B type LiFePO₄ battery cell [13].

$$\hat{R}_s = \hat{\delta}/\hat{\sigma} \quad (32a)$$

$$\hat{C}_c = -\frac{1 + \hat{\mu} C_s \hat{R}_s + \hat{\delta} C_s^2 \hat{R}_s}{\hat{\delta} C_s \hat{R}_s} \quad (32b)$$

$$\hat{R}_c = \frac{1}{\hat{\delta} \hat{C}_c C_s} \quad (32c)$$

4. Experimental results and validation for battery cell and stack model

4.1. Experiment setup

The experiment tests are conducted on a LiFePO₄ battery cell of type ANR26650M1-B to validate the proposed electro-thermal model. The entire experiment setup is shown in Fig. 6. In Section 3, the standard CC-CV test is performed to identify the electrical model. The voltage for the cell varies from 2.5 V to 3.6 V with the cut-off current value of around 0.05A. The entire test is repeated at different ambient temperatures such as 5 °C, 15 °C, 25 °C, 35 °C and 45 °C inside the climatic chamber (Weiss WKL 34/70) to obtain the temperature-dependent parameters. The current is generated by a direct-current (DC) electronic load (KIKUSUI PLZ1004W) while the battery cells are charged by a programmable DC power supply (GwINSTEK GPC-30600) to control the voltage (maximum at 36 V) and current (maximum at 20A). The host computer links between the data acquisition (DAQ) device and the battery cell. The DAQ device then controls the input and output data with the acquisition rate set as 1 Hz. A current sensor measures the current. A K-type thermocouple is placed on the surface of the battery cell and temperature data was logged by a data acquisition unit (KEYSIGHT 34972A) to measure the surface temperature of the cell. An infrared thermal camera (FLUKE Ti400) [13] is used to obtain the

thermal images that are processed by FLUKE's SmartView infrared imaging analysis and reporting software.

4.2. Results in electrical model parameterization

Since the tests are conducted at different ambient temperatures to obtain the temperature-dependent parameters in R_0 , R_1 , and C_1 at each SOC. The current, SOC and voltage for the discharge of the battery cell can be seen in Fig. 7. The SOC and temperature are constant during the relaxation for R_0 , R_1 and C_1 identification at a different fixed temperature. Although the charging of the battery cell is not conducted, based on the results shown [23], R_0 remains quite constant at different SOC. The parameter values used in (23) can be different. The value of R_0 is determined by evaluating the instantaneous jump in the voltage after the current pulse using Ohm's law as seen in Fig. 7.

The mean values of the R_0 are evaluated for each SOC value. As observed in R_0 vs SOC shown in Fig. 8, R_0 remains quite independent at different SOC values (0.1 to 0.9).

$$R_{0,5^{\circ}\text{C}} = -0.0058\text{SOC} + 0.096 \quad (33a)$$

$$R_{0,15^{\circ}\text{C}} = -0.0037\text{SOC} + 0.090 \quad (33b)$$

$$R_{0,25^{\circ}\text{C}} = -0.0031\text{SOC} + 0.084 \quad (33c)$$

$$R_{0,35^{\circ}\text{C}} = 0.0014\text{SOC} + 0.071 \quad (33d)$$

$$R_{0,5^{\circ}\text{C}} = 0.0016\text{SOC} + 0.070 \quad (33e)$$

As seen in Fig. 8, the maximum deviation of R_0 at 5 °C, 15 °C, 35 °C and 45 °C are around 0.0065Ω, 0.0050Ω, 0.0055Ω, 0.0030Ω, 0.0050Ω, respectively. However, it shows a strong dependence on the temperature. To show this, a mean value is used to represent R_0 at the different ambient temperatures. As the temperature increases, the value of R_0 decreases as seen in Fig. 9. It reduces by a value of 0.0214 Ω from 5 °C to 30 °C and remains quite constant at 35 °C and 45 °C. This phenomena is due to the high active reaction kinetics [23] at higher temperature as shown below.

$$R_0 = 0.0976e^{-0.0077T_a} \quad (34)$$

As observed in Fig. 10, the value of R_0 can deviate around 0.0800 Ω for different LiFePO4 cell operating in different temperature. The same pulse test is repeated for the different cells under same temperature. The R_0 decreases as the temperature increases. In Table 2, the mean values of R_0 at different ambient temperatures are tabulated. It can be seen that the mean absolute error is around 0.0694 Ω. The error is smaller at higher temperature. By comparing the R_0 values obtained in the literature, the values are different due to the higher pulse current of 2.5 A [23] and 3 A [27] used to identify the electrical model parameters (as compared to 2 A used in this paper). In addition, the current age or state-of health (depends on the number of charge and discharge cycle) of the cell can affect the results. As seen in Fig. 9, R_0 value can deviate more than 0.0800 Ω across different cells with the mean absolute error

of 0.0694 Ω. Since the heat generation, Q is approximated as the product of the squared current and lumped resistance, the heat generation can be higher at lower temperature as a lower temperature increases the resistance (that could also reduce the cell's capacity in Ah).

The R_1 and C_1 parameter is obtained by minimizing the voltage least square error in (26). Different behavior can be observed in Fig. 11. Typically, the value of R_1 increases with higher temperatures. In the case of SOC, R_1 is quite high for a high SOC value. The R_1 demonstrates less dependence on SOC except when it reaches more than 80%. The discharge resistance is generally lower when SOC drops to below 80%. However, such dependence should be opposite for the case of charge resistance. Instead of using the Arrhenius-like function [23] to include the temperature dependency, a separate polynomial function to include temperature dependency is used.

$$R_1(\text{SOC}) = (5.2\text{SOC}^3 - 6.4\text{SOC}^2 + 2\text{SOC} - 0.1) \times 10^{-3} \quad (35a)$$

$$R_1(T_a) = (2.5 \times 10^{-5}T_a^2 + 0.002T_a + 0.06) \times 10^{-3} \quad (35b)$$

However, C_1 exhibits a fluctuating behavior with a few maximum and minimum points as seen in

Fig. 11. The relationship between SOC and C_1 are quite complex as compared to R_1 . The values of C_1 is curve fitted using sinusoidal based functions that have similar fluctuating behavior. Another third-order polynomial function is used to include the temperature dependence term in C_1 . In general, the value of C_1 increases with higher temperatures.

$$C_1(\text{SOC}) = 4.21 \times 10^3 \sin(2.3\text{SOC} + 0.7) + 2.12 \times 10^3 \sin(24\text{SOC} - 0.7) + 2.835 \times 10^3 \sin(21\text{SOC} - 1.4) \quad (36a)$$

$$C_1(T_a) = -0.465T_a^3 + 42T_a^2 - 1010T_a + 9400 \quad (36b)$$

It is not meaningful to use a constant value of R_1 and C_1 to represent the RC parameter of the electrical circuit as the values changes with SOC and temperature. Despite of that, the value of $R_1 = 0.004 \Omega$ [27] and $C_1 = 156\text{F}$ [27] at 25 °C was used. As compared to Table 3 at a different temperature, the values are quite different from the values [27]. In Fig. 12, the voltage mean square error (MSE) ranges from 0.0252 V to 0.0311 V when compared to the experimental results. The MSE is greater at a higher and lower temperature. The MSE of terminal voltage is less than 0.02 V. The error is caused by the actual load current was slightly lower than the 2A used in the simulation.

In Fig. 13, the terminal voltage increases at higher ambient temperature and decreases at lower ambient temperature. Although the terminal voltage is determined using the pulse current rate of 2 A, similar behavior can be obtained at a different load current.

The terminal voltage estimated by the electrical model can be seen in Fig. 14. The plots compared the simulated model using an ambient temperature-dependent and independent electrical model with the experimental results. For brevity, only the terminal voltage at the lowest and highest temperature of 5 °C and 45 °C are shown. The RMSEs at different temperatures are tabulated in Table 4. The results shown that

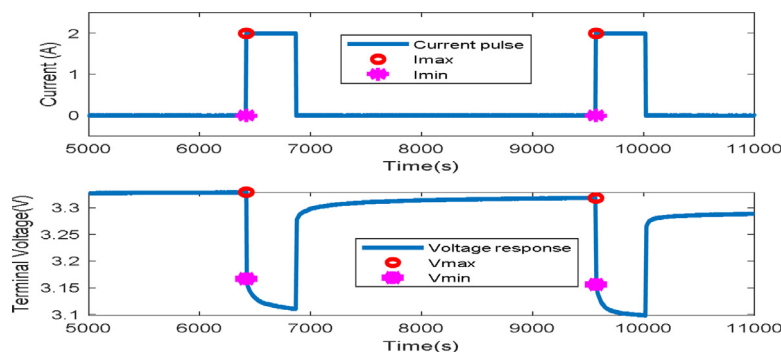
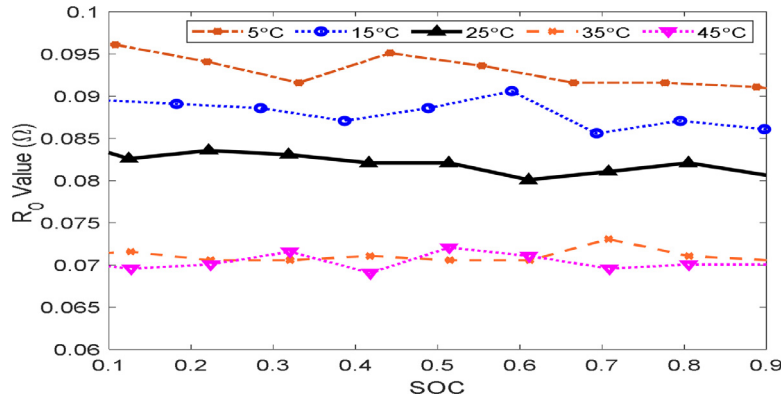


Fig. 7. Evaluating R_0 based on the instantaneous jump in voltage and current of 2A.

Fig. 8. R_0 vs SOC for discharging at different ambient temperature.

the temperature-dependent model exhibits a maximum RSME of 0.1764 V as compared to the temperature independent model of 0.4183 V. On the other hand, the temperature-independent model is obtained using only the parameters obtained at 25 °C. In general, the terminal voltage RMSE is lower than 0.2 V. The RMSE is greater at a higher and lower temperature.

For the open-circuit voltage (U_{oc}), it is obtained from the terminal voltage at its equilibrium (see Fig. 5). The value U_{oc} depends on SOC value. A logarithm function in (3) is used to compute the OCV for each SOC. The relationship between OCV and SOC can be seen in Fig. 15.

$$U_{oc}(SOC) = 3.44 - 0.191SOC + 0.108\ln(SOC) - 0.033\ln(1 - SOC) \quad (36)$$

As seen in Fig. 15, U_{oc} depends on the ambient temperature. However, U_{oc} remains independent with ambient temperature at SOC (0.3 to 0.95). A slightly high variation can occur at lower temperatures such as 5 °C and 15 °C.

4.3. Estimation of nonlinear function

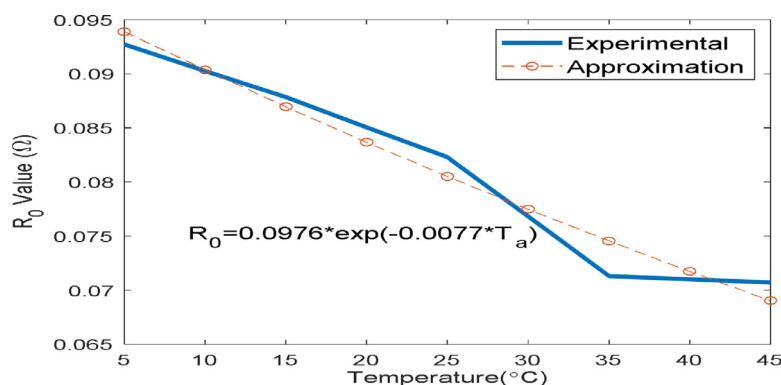
The nonlinearities term, $f(SOC, I)$ in (9) can be estimated based on the input pulsed current, experimental data of SOC and OCV-SOC relationship. As seen in Fig. 16, the value drops to around -250 before it start to converge to -0.8 over the simulation time. In general, the nonlinear term reduces the rate of change of the terminal voltage value by around -0.8.

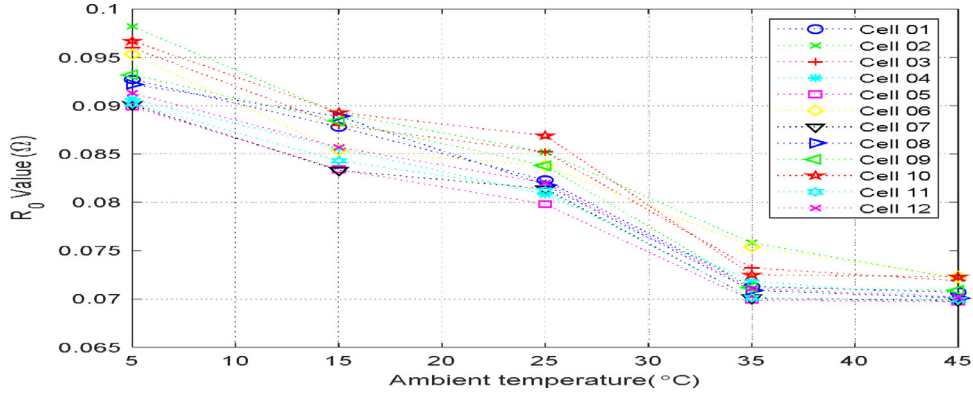
4.4. Results of thermal model parameters

The thermal model is obtained from the data collected using the experimental setup in Fig. 6. The measured ambient temperature T_a , pulse, constant current $I = 10A$ and surface temperature of the cell, T_s are plotted in Fig. 16. The surface temperature exceeds the temperature

of the cell surface. By using $C_s = 4.5 \text{ J/K}$, the identified R_c , C_c , and R_s can be tabulated in Table 5. The parameters are quite close to the values [17,23,37]. The maximum variation of the thermal parameters can be determined by examining the estimated value and values from the literature. It exhibits a different of 15.3 J/K and 6.07 k/W in C_c and R_s , respectively. Using the lumped resistance R_d , the heat generation can be computed as $Q = I^2R_d$. The lumped value of the resistance consists of the heat dissipation in R_0 and the RC circuit. As shown in R_0 and R_1 in Tables 2 and 3, respectively, the combined value of R_d is 0.0833Ω at 25 °C. The value is quite different from 0.0114Ω as identified [23] on the same type of cell. The change in entropy of the battery cell is not included in (11) that can produce an error in the computation of heat generation. Additionally, the value of R_d could vary [17] and depend on SOC, temperature and the age of the battery cell. With that, the R_d values at different temperatures can be used.

The load current of 10 A together with the measured T_a and T_s in Fig. 17 are used in the least square approach. The simulated surface temperature shows a maximum error of 1.2 K as seen in Fig. 16. The initial values of the parameters are namely: $R_c = 4.0 \text{ k/W}$, $R_s = 6.0 \text{ k/W}$ and $C_c = 80 \text{ J/K}$. Note that the single C_p [7] consists of both C_s and C_c . The heat capacities depend on the weight of the electrode assembly, thermal properties and the casing of the cell. They are quite constant over time. The heat capacities can affect the transient response of the model without affecting the temperatures in a steady-state. The heat capacity of C_c is estimated as 71.5 J/K while C_s is assumed as 4.5 J/K based on the specific heat capacity of aluminum and the size of the battery cell. The combined $C_p = 76 \text{ J/K}$ is slightly higher than $C_p = 73.2 \text{ J/K}$ found in [7] for different current pulses of 20A of the same battery cell. As shown in Fig. 17, the difference between the surface and ambient temperature is around 3.6 K for 10A. Similar phenomena can be seen in the thermal map of the cell's surface in Fig. 17 where the error between the simulation and measurement (both using thermocouple and thermal camera) is around 0.5 K.

Fig. 9. Approximation of R_0 vs ambient temperature during discharging .

Fig. 10. R_0 value at different ambient temperature across 12-cell of LiFePO₄ cell.**Table 2**

Mean value of R_0 at different ambient temperatures as compared with equivalence found in literature.

Measured R_0 (in Ω)				
5 °C	15 °C	25 °C	35 °C	45 °C
0.0927	0.0878	0.0823	0.0713	0.0707
Equivalence R_0 (in Ω)				
0.0190 [23]	0.0135 [23]	0.010 [27]	0.0090 [23]	0.0082 [23]
		0.011 [23]		
Absolute error of R_0 (in Ω) [mean across temperatures: 0.0694 Ω]				
0.0737	0.0743	0.0723	0.0623	0.0625
		0.0713		

The heat capacity and resistance of the thermal model namely: C_c , C_s , R_c , R_s are used to investigate the sensitivity [18] of the parameters to the changes on the surface and core temperature of the cell. As seen in Table 5, the thermal parameters can vary in different literature and the type of cell used. Thus, the parameters are sequentially perturbed using -30% to $+30\%$ of the estimated value while keeping other parameters constant. In the simulation, the load current of 10 A is used. Fig. 18 indicates that the resistance of conduction R_c has more impact on the core temperature than the surface temperature. It implies that the heat transfer is indeed at conduction mode. Conversely as seen in Fig. 19, the resistance of convection R_s affects the surface temperature more than the core temperature as it can be quite sensitive to changes in the resistance of convection due to the convective heat transfer.

As seen in Fig. 20, the heat capacity for conduction, C_c can affect the

Table 3

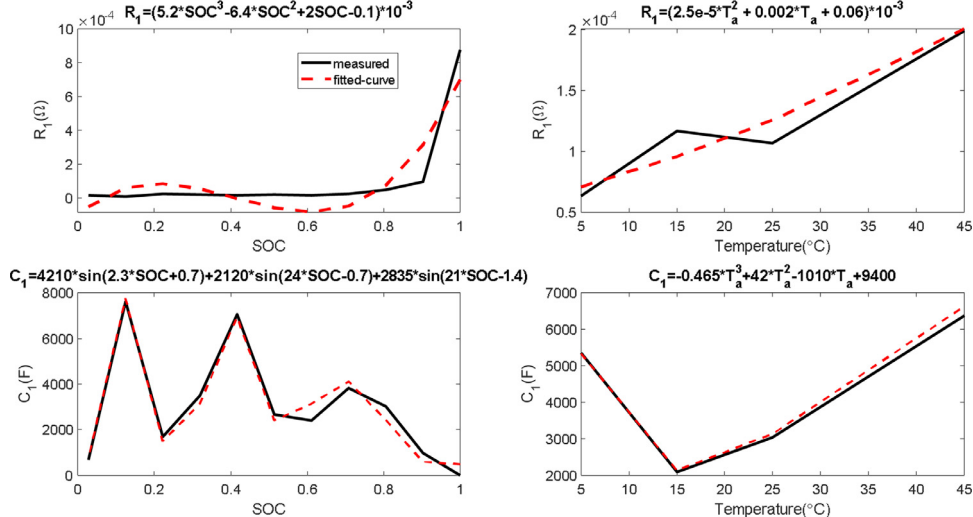
Mean value of RC parameters and MSE of terminal voltage at different ambient temperatures .

	5 °C	15 °C	25 °C	35 °C	45 °C
$R_1(\Omega)$	0.00063	0.00116	0.00106	0.00112	0.00198
$C_1(F)$	5346	2088	3039	3475	6382
Terminal Voltage MSE (V)	0.0308	0.0252	0.0311	0.0268	0.0307

transient response of the surface and core temperature without affecting the temperatures at the steady-state. On the other hand, the heat capacity for convection, C_s has the least effect on the core temperature of the cell as there is no convection at the core in Fig. 21. However, the surface temperature follows the same behavior except at a higher uncertainty of $+20\%$ and $+30\%$.

4.5. Results of sensitivity test on thermal model

In summary, the root mean square error (RMSE) of the thermal parameters, C_c , C_s , R_c , R_s from its nominal values are varied at $\pm 30\%$ (see Fig. 22). The heat capacity and resistance of convection have more influence on the estimation of the surface and the core temperatures than the conduction (that exhibits less dependent on core and surface temperature [7,16,44]). The core temperature is higher than the surface temperature as heat is dissipated from its core to the surface via conduction followed by convection to the surrounding. The difference between the surface and core temperature (based on the

Fig. 11. R_1 and C_1 value at different SOC and ambient temperature .

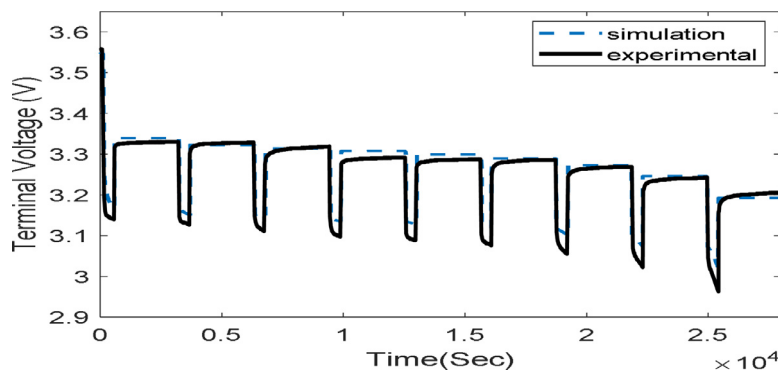


Fig. 12. Terminal voltage response for RC parameter at 25 °C.

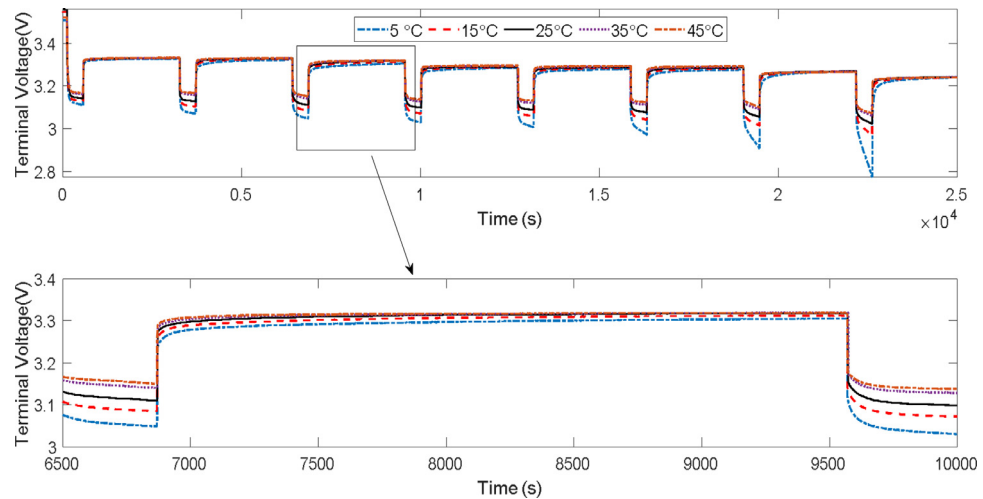


Fig. 13. Terminal voltage response for RC parameter at different temperatures .

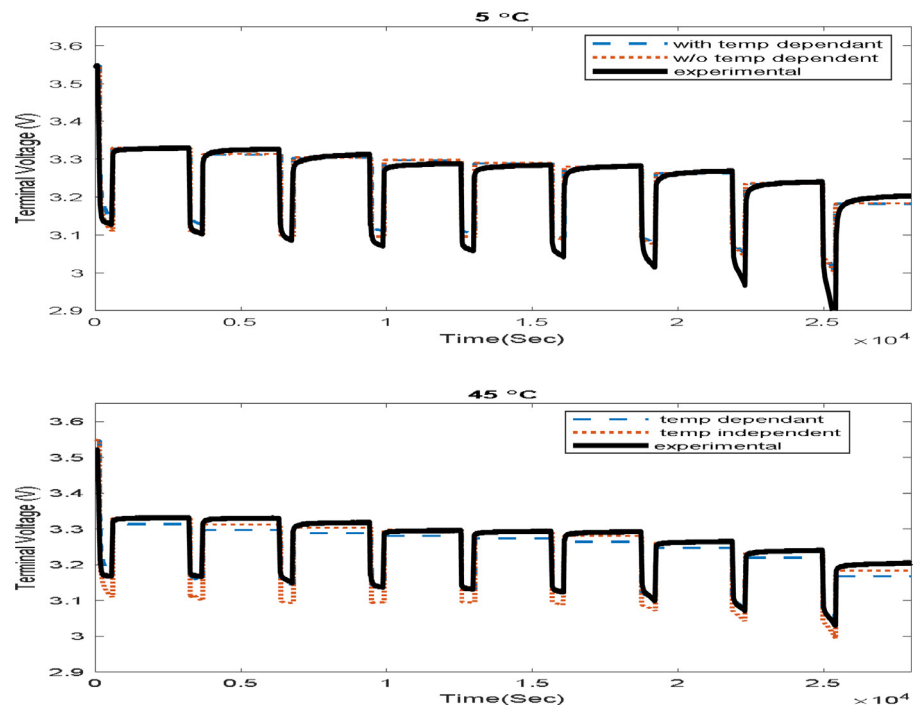


Fig. 14. Simulated terminal voltage response at 5 °C (top) and 45 °C (bottom) as compared to experiment.

Table 4

Comparison of terminal voltage RMSE at different ambient temperature to experiment (with and without temperature dependent).

	Terminal Voltage RMSE (in V)				
	5 °C	15 °C	25 °C	35 °C	45 °C
Temperature dependant	0.1754	0.1586	0.1764	0.1637	0.1751
Temperature independant (using parameters at 25 °C)	0.4170	0.4183	0.1764	0.4171	0.4174

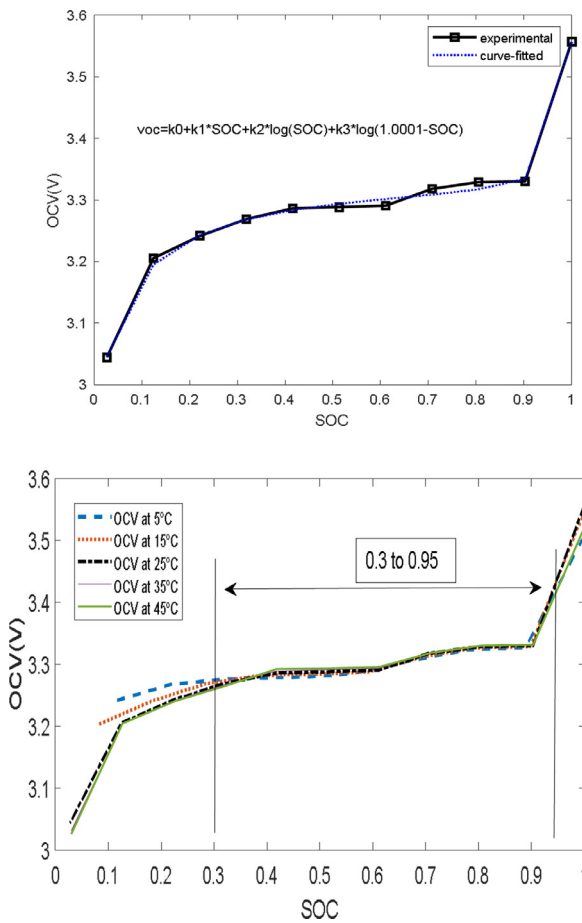


Fig. 15. OCV vs SOC(left) and its ambient temperature dependency (right) .

Table 5

Value of thermal parameters as compared with equivalence found in literature.

Thermal Parameters	Estimated Value	Equivalence			Maximum Variation
		Ref. [23]	Ref. [17]	Ref. [40]	
R_c (k/W)	2.23	1.94	1.83	3.2~3.4	1.57
R_s (k/W)	4.35	3.19	3.03	8.4~9.1	6.07
C_s (J/K)	4.50	4.50	4.50	-	4.50
C_c (J/K)	71.5	62.7	67.0	73~78	15.3

nominal value) is around 2 K. The results also indicate that the heat capacity C_c and C_s parameters can assume constant due to the parametric changes to the steady-state value is negligible. Also, the convection resistance, R_s depends on the surrounding temperature that affects the accuracy of the core and surface temperature estimation of the battery cell more than other parameters in the thermal model.

4.6. Results of electro-thermal battery stack model

The electro-thermal battery stack model is derived in Section 2 and the parameters can be obtained from Section 4. Fig. 23 shows the setup to determine the surface temperature of each cell. A total of twelve cells are contacted in series where the positive side of the cell is connected to the negative end of the next cell. The cells are placed on an acrylic fixture where they are positioned properly to hold the cells under natural convection. The K-type thermocouples are used to measure the surface temperature of each cell. The thermocouples are used to measure the surface temperature of each cell. They are placed underneath the cells (for clarity as the topside consists of many wires). The core temperature is not measured. The heat generation are assumed to be constant for each cell.

As seen in (18), the temperature gain factor is determined using the thermal conductivity of $K_c = 0.488 \text{ W/m.K}$ and convection coefficient of $h = 5 \text{ W/m}^2\text{K}$ used [18,38,46]. The value of $\Delta K = 0.026 \text{ K/W}$ is obtained where the cell radius, $R_1 = 0.013 \text{ m}$ and the ratio $R_2/R_1 = 3$. The pulsed current of $I = 2\text{A}$ and the constant heat generation, Q is computed. As observed in Fig. 24, the surface temperatures at each cell can be estimated. The surface temperature increases linearly from cell #1 to #12 under the constant heat generation of each cell $#i$. The thermal model shows a good match with the surface temperature measurements obtained from the K-type thermocouples. The RMSE between the surface measurement and model of the battery stack is around 3 °C.

On the other hand, the core temperatures for each cell are shown in Fig. 24. The core temperatures are slightly lower than the surface temperatures when the cells are placed in a stack. It can be attributed to the synergized effects [46] of higher local temperature and local current when placed near to one another. It causes a higher conductive heat

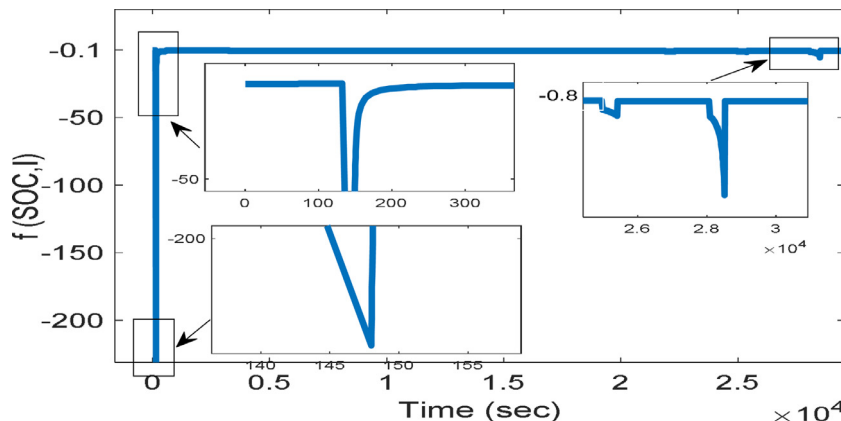


Fig. 16. Nonlinearities term based on current, experimental data of SOC and OCV-SOC relationship.

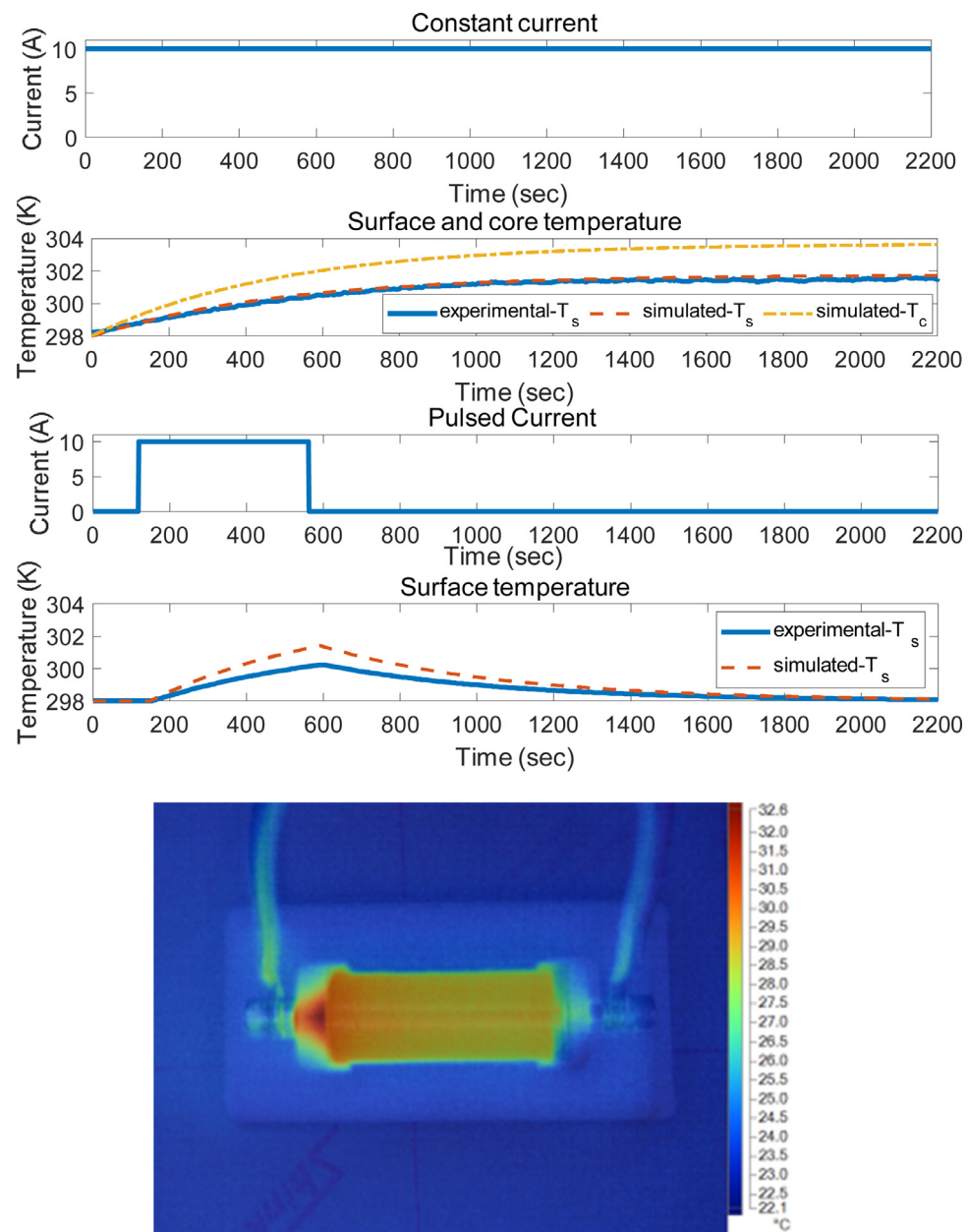


Fig. 17. Measured surface and simulated core temperature of LiFePO₄ cell at fixed (top), pulsed current (middle) and thermal image of cell surface (bottom) at 10 A.

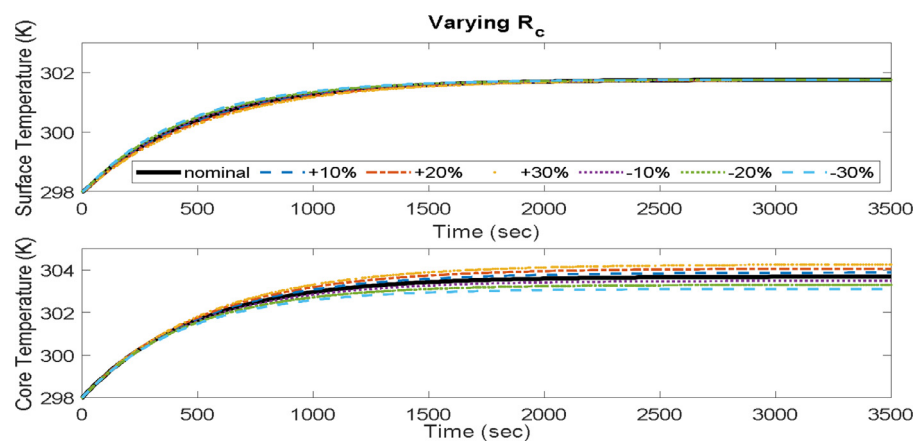


Fig. 18. Variation of R_c on core and surface temperature estimation under -30% to +30% uncertainty.

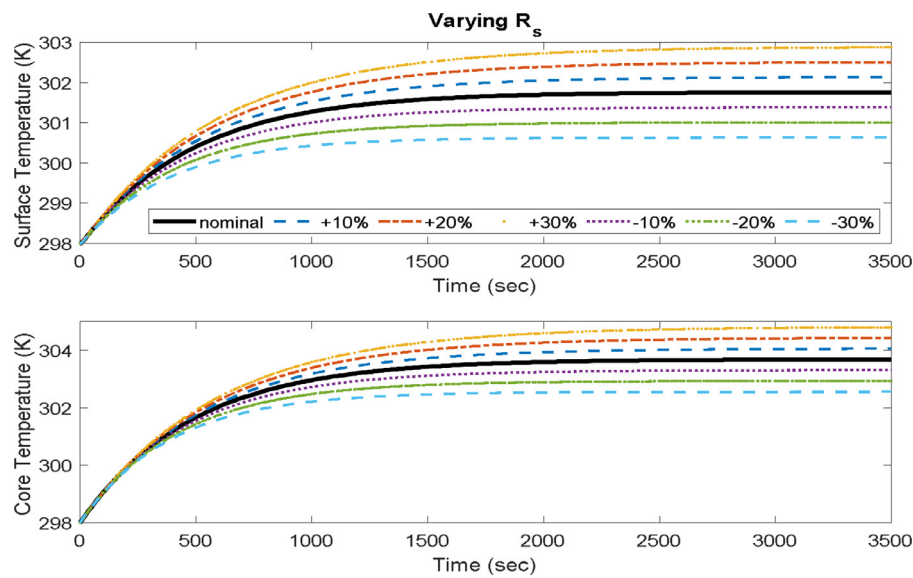


Fig. 19. Variation of R_s on core and surface temperature estimation under -30% to $+30\%$ uncertainty.

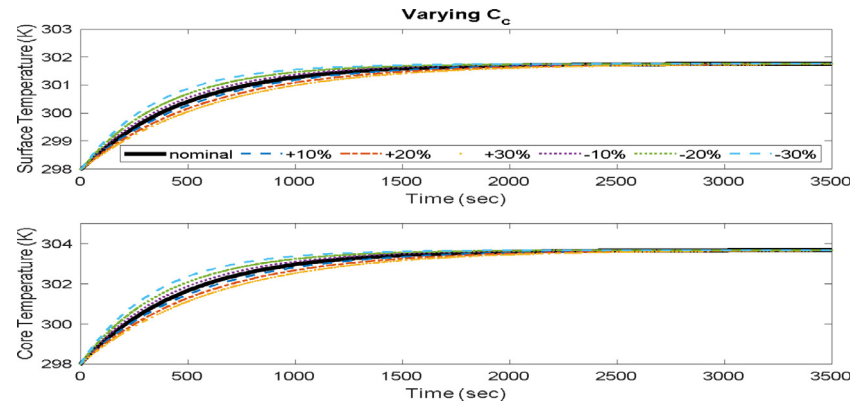


Fig. 20. Variation of C_c on core and surface temperature estimation under -30% to $+30\%$ uncertainty.

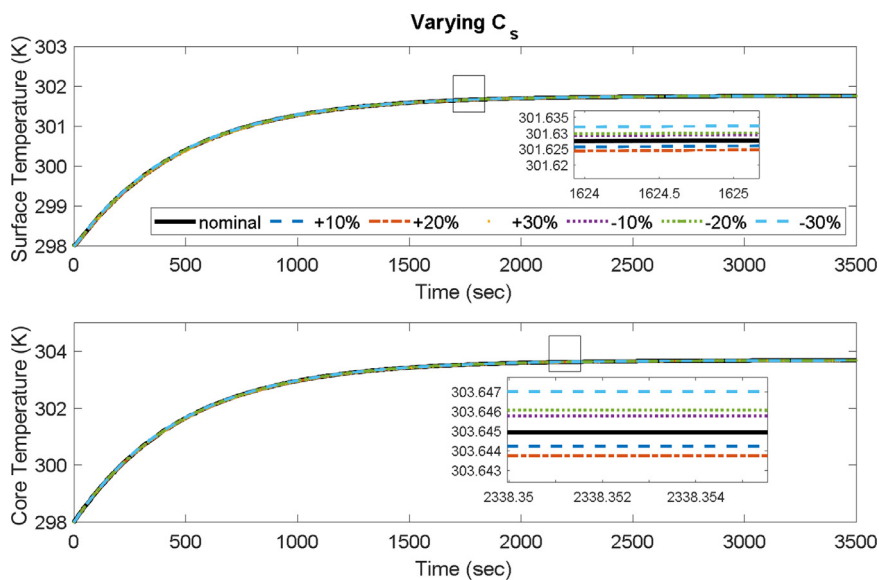


Fig. 21. Variation of C_s on core and surface temperature estimation under -30% to $+30\%$ uncertainty.

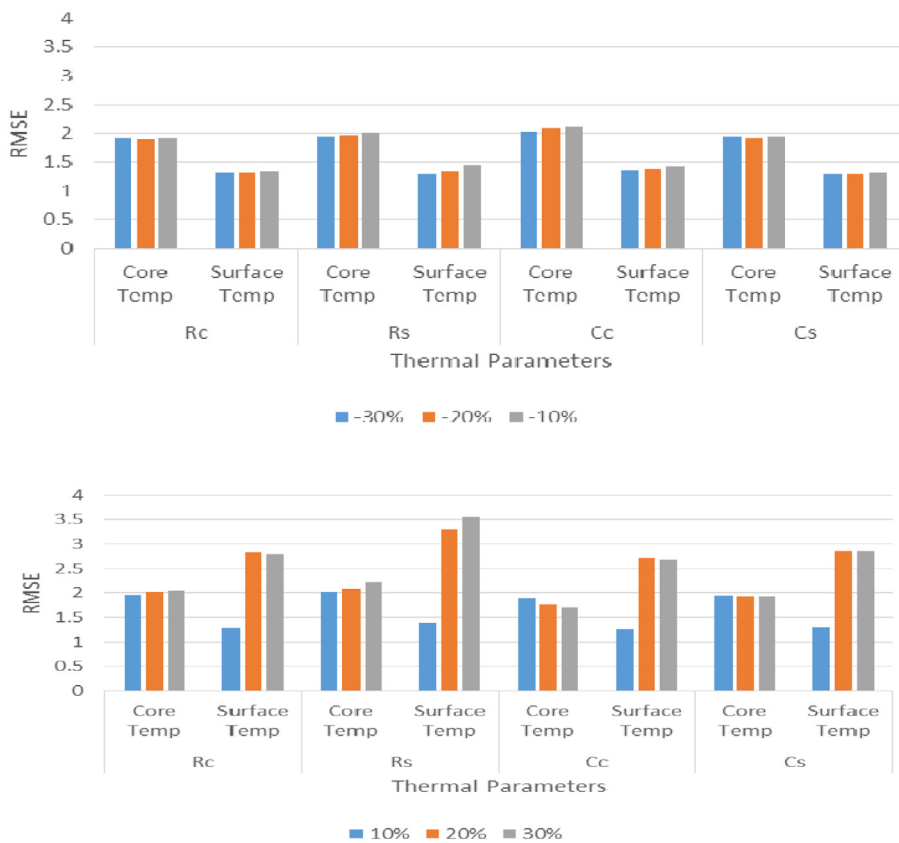


Fig. 22. RMSE of core and surface temperatures under -30% to -10% (top) and $+10\%$ to $+30\%$ (bottom) uncertainty in CC , Cs , Rc , Rs .

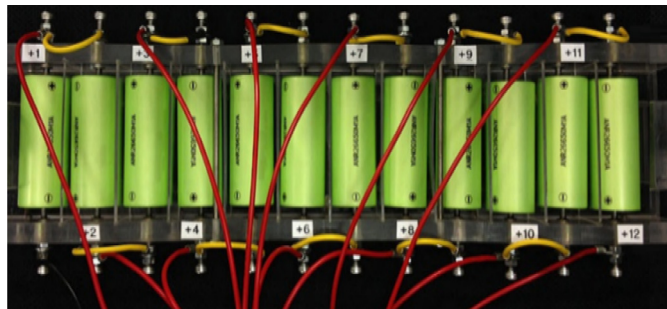


Fig. 23. Actual setup of LiFePO₄ cells in series to form battery stack (with thermocouples at the back of cells not shown for clarity).

transfer when the cells are connected in series, resulting in lower core temperature. In addition, a smaller cell such as LiFePO₄ ANR26650M1-B has a better temperature distribution. By varying K_c and h by $+/ - 30\%$, the surface temperatures of the cells can deviate as seen in Fig. 25. The surface temperature increases as K_c and h decreases. In Fig. 24, the surface temperature increases from cell #1 to #12. The RMSE of the battery cells under different uncertainties is different as shown in Fig. 25.

The RMSE of the surface temperature as compared to the nominal value is higher at -30% than $+30\%$. At lower uncertainty such as $+10\%$ and $+20\%$, the RMSE is lower than the thermal model uncertainty at -30% and -20% . Similar phenomena can be observed in the core temperature when the thermal parameters are perturbed by $+/ - 30\%$.

In summary, the accurate modeling of the cell temperatures is important in battery health monitoring. It is known that the internal resistance increases, the temperatures can increase due to higher heat generated. Despite the core and surface temperature are identified, the electro-thermal cell model can become less accurate due to the cells' aging. By updating the parameter of R_0 and RC pair, it can improve the

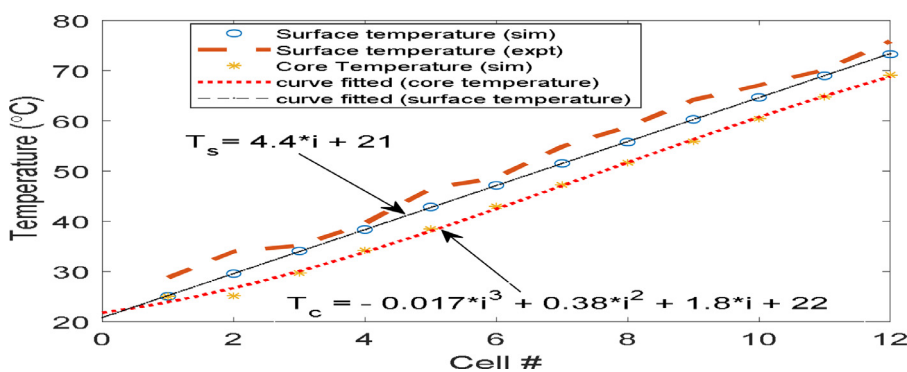


Fig. 24. Simulated surface and core temperature of each LiFePO₄ cell in battery stack with comparison with experimental results for surface temperature.

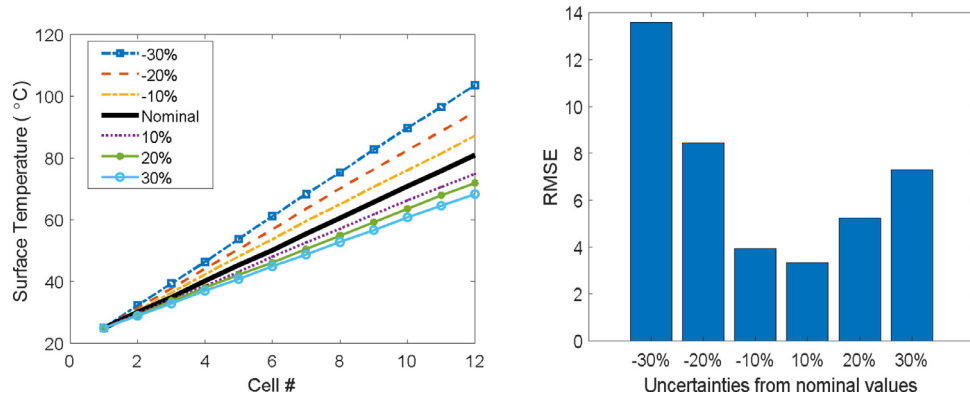


Fig. 25. Surface temperature of each LiFePO4 cell (left) and RMSE under -30% to $+30\%$ uncertainty in K_c and h (right).

voltage estimation accuracy. Although updating the parameters can produce better results, it can be quite challenging for actual implementation as the BMS consumes higher computation resources and cost over the lifetime of the battery in actual applications.

5. Conclusion

This paper presented the coupled electro-thermal state-space model to predict both the surface and core temperature of the cell and battery stack. The coupling between the electrical and thermal model enables estimation of the voltages and temperatures under uncertainties due to the thermal parameters using measurable inputs such as voltage, current, and ambient temperature. The internal resistance and resistor-capacitor (RC) model of the electrical model at different ambient temperatures such as $5\text{ }^\circ\text{C}$, $15\text{ }^\circ\text{C}$, $35\text{ }^\circ\text{C}$ and $45\text{ }^\circ\text{C}$ and SOC levels were identified. The relationships between the electrical parameters such as state-of-charge (SOC) and open-circuit voltage were obtained at various ambient temperature levels. The main results for the battery cell can be summarized as shown.

- The open-circuit voltage remains quite independent with ambient temperature at SOC value between 0.3 to 0.95 at $5\text{ }^\circ\text{C}$ and $15\text{ }^\circ\text{C}$.
- The thermal parameters such as R_c , C_c , and R_s were identified as 2.23 k/W , 71.5 J/K and 4.35 k/W , respectively. The variation of the core and surface temperature of the cell was quite high for R_s (in both transient and steady-state) and C_c (in steady-state only). The value of R_s depends on the surrounding temperature affecting the accuracy of the core and surface temperature estimation more than other parameters.
- The difference between the surface and ambient temperature was around 3.6 K as compared to the temperature between the core and surface of around 2 K .

For the battery stack, the following results were obtained.

- Root mean square error of the surface temperature between the measurement and simulation of the battery stack was around $3\text{ }^\circ\text{C}$.
- The core temperatures exhibited slightly lower surface temperatures as all cells were placed in a stack causing higher conductive heat transfer among the cells resulting in the lower core temperature.

Future works will include the aging of cells in battery stack over wider operating temperatures in multiple electric vehicles. The experimental uncertainty analysis and hybrid pulse power characterization (HPPC) test will be performed to improve the accuracy of the model.

CRediT authorship contribution statement

C.S. Chin: Conceptualization, Formal analysis, Funding acquisition, Writing - review & editing, Project administration. **Z. Gao:** Data curation, Resources, Software, Writing - original draft. **C.Z. Zhang:** Validation, Visualization, Supervision.

Declaration of Competing Interest

None.

Supplementary materials

Supplementary material associated with this article can be found, in the online version, at doi:[10.1016/j.est.2020.101222](https://doi.org/10.1016/j.est.2020.101222).

References

- [1] Z. Yang, D. Patil, B. Fahimi, Electrothermal modeling of lithium-ion batteries for electric vehicles, *IEEE Trans. Vehicul. Technol.* 68 (1) (2019) 170–179.
- [2] J. Zhang, L. Zhang, F. Sun, Z. Wang, An overview on thermal safety issues of lithium-ion batteries for electric vehicle application, *IEEE Access* 6 (2018) 23848–23863.
- [3] C. Vidal, O. Gross, R. Gu, P. Kollmeyer, A. Emadi, xEV li-ion battery low-temperature effects—review, *IEEE Trans. Vehicul. Technol.* 68 (5) (2019) 4560–4572.
- [4] D. Tenfen, E.C. Finardi, B. Delinchant, F. Wurtz, Lithium-ion battery modeling for the energy management problem of microgrids, *IET Gener. Transm. Distrib.* 10 (3) (2016) 576–584.
- [5] F. Ye, Y. Qian, R.Q. Hu, Incentive load scheduling schemes for PHEV battery exchange stations in smart grid, *IEEE Syst. J.* 11 (2) (2015) 922–930.
- [6] L.C. Casals, B.A. Garca, Communications concerns for reused electric vehicle batteries in smart grids, *IEEE Communications Magazine* 54 (9) (2016) 120–125.
- [7] C. Forgez, D.V. Do, G. Friedrich, M. Morcrette, C. Delacourt, Thermal modeling of a cylindrical lifepo4/graphite lithium-ion battery, *J Power Sources* 195 (2010) 2961–2968.
- [8] P.M. Gomadam, R.E. White, J.W. Weidner, Modeling heat conduction in spiral geometries, *J. Electrochem. Soc.* vol.150, (10) (2003) A1339–A1345.
- [9] S. Al-Hallaj, H. Maleki, J.S. Hong, J.R. Selman, Thermal modeling and design considerations of lithium-ion batteries, *J Power Sources* 83 (1–2) (1999) 1–8.
- [10] S.A. Khateeb, S. Amiruddin, M. Farid, J.R. Selman, S. Al-Hallaj, Thermal management of Li-ion battery with phase change material for electric scooters: experimental validation, *J. Power Source.* 142 (1–2) (2005) 345–353.
- [11] K. Smith, C.Y. Wang, Solid-state diffusion limitations on pulse operation of a lithium ion cell for hybrid electric vehicles, *J. Power Source.* vol.160, (1) (2006) 662–673.
- [12] G.H. Kim, A. Pesaran, R. Spotnitz, A three-dimensional thermal abuse model for lithium-ion cells, *J. Power Source.* 170 (2) (2007) 476–489.
- [13] J. Chiew, C.S. Chin, W.D. Toh, Z. Gao, J. Jia, C.Z. Zhang, A pseudo three-dimensional electrochemical-thermal model of a cylindrical LiFePO4/graphite battery, *Appl. Therm. Eng.* 147 (2019) 450–463.
- [14] H. Maleki, S.A. Hallaj, J.R. Selman, R.B. Dinwiddie, H. Wang, Thermal properties of lithium-ion battery and components, *J. Electrochem. Soc.* 146 (3) (1999) 947–954.
- [15] S.C. Chen, C.C. Wan, Y.Y. Wang, Thermal analysis of lithium-ion batteries, *J. Power Source* 140 (1) (2005) 111–124.
- [16] K. Onda, T. Ohshima, M. Nakayama, K. Fukuda, T. Araki, Thermal behavior of small lithium-ion battery during rapid charge and discharge cycles, *J. Power Source* 158 (1) (2006) 535–542.
- [17] X. Lin, H.E. Perez, J. Siegel, A. Stefanopoulou, Y. Li, R.D. Anderson, Y. Ding, M.P. Castanier, On-line parameterization of lumped thermal dynamics in cylindrical

- lithium ion batteries for core temperature estimation and health monitoring, *IEEE Trans. Control Syst. Technol.* 21 (2013) 1745–1755.
- [18] Y. Kim, S. Mohan, J.B. Siegel, A.G. Stefanopoulou, Y. Ding, The estimation of temperature distribution in cylindrical battery cells under unknown cooling conditions, *IEEE Trans. Control Syst. Technol.* vol.22, (6) (2014) 2277–2286.
- [19] Z. Wang, J. Ma, L. Zhang, Finite element thermal model and simulation for a cylindrical Li-ion battery, *IEEE Access* 5 (2017) 15372–15379.
- [20] S. Dey, H.E. Perez, S.J. Moura, Model-based battery thermal fault diagnostics: algorithms, analysis, and experiments, *IEEE Trans. Control Syst. Technol.* 27 (2) (2019) 576–587.
- [21] X.B. Meng, H.X. Li, H.D. Yang, Evolutionary design of spatio-temporal learning model for thermal distribution in lithium-ion batteries, *IEEE Trans. Ind. Inform.* 15 (5) (2019) 2838–2848.
- [22] D.H. Jeon, S.M. Baek, Thermal modeling of cylindrical lithium ion battery during discharge cycle, *Energy Convers. Manag.* 52 (8–9) (2011) 2973–2981.
- [23] X. Lin, H.E. Perez, S. Mohan, J.B. Siegel, S. A.G, Y. Ding, A lumped parameter electro-thermal model for cylindrical batteries, *J. Power Source.* 257 (2014) 1–11.
- [24] C. Zou, X. Hu, Z. Wei, X. Tang, Electrothermal dynamics-conscious lithium-ion battery cell-level charging management via state-monitored predictive control, *Energy* 141 (2017) 250–259.
- [25] M. Chen, G.A.R. Mora, Accurate electrical battery model capable of predicting runtime and I–V performance, *IEEE Trans. Energy Convers.* 21 (2) (2006) 504–511.
- [26] S. Wijewardana, R. Vepa, M.H. Shaheed, Dynamic battery cell model and state of charge estimation, *J Power Sources* 308 (2016) 109–120.
- [27] W. Chen, W.T. Chen, M. Saif, M.F. Li, H. Wu, Simultaneous fault isolation and estimation of lithium-ion batteries via synthesized design of Luenberger and learning observers, *IEEE Trans. Control Syst. Technol.* 22 (1) (2014) 290–298.
- [28] F. Sun, R. Xiong, H. He, Estimation of state-of-charge and state-of-power capability of lithium-ion battery considering varying health conditions, *J. Power Source.* 259 (2014) 166–176.
- [29] J. Jaguemont, N.O. A.Nikolian, S. Goutam, J.V. Mierlo, P.V.D. Bossche, Development of a two-dimensional-thermal model of three battery chemistries, *IEEE Trans. Energy Convers.* 32 (4) (2017) 1447–1455.
- [30] M. Alhanouti, M. Gießler, T. Blank and F. Gauterin, New electro-thermal battery pack model of an electric vehicle, *Energies*, vol. 9, no. 563, 2016.
- [31] L.H. Saw, Y. Ye, A.A.O. Tay, Electro-thermal analysis and integration issues of lithium ion battery for electric vehicles, *Appl. Energy* 131 (15) (2014) 97–107.
- [32] Y. Hu, S. Yurkovich, Y. Guezennec, B.J. Yurkovich, Electro-thermal battery model identification for automotive applications, *J. Power Source.* 196 (1) (2011) 449–457.
- [33] A. Farnmann, W. Waag, D.U. Sauer, Adaptive approach for onboard impedance parameters and voltage estimation of lithium-ion batteries in electric vehicles, *J. Power Source.* 299 (0) (2015) 176–188.
- [34] Z. Li, J. Huang, B.Y. Liaw, J. Zhang, On state-of-charge determination for lithium-ion batteries, *J. Power Source.* 348 (2017) 281–301.
- [35] S. Panchal, J. McGrory, J. Kong, I. Dincer, M. Agelin-Chaab, R. Fraser, M. Fowler, Cycling degradation testing and analysis of a LiFePO₄ battery at actual conditions, *Int. J. Energy Res.* 41 (15) (2017) 2565–2575.
- [36] S. Panchal, I. Dincer, M. Agelin-Chaab, R. Fraser, M. Fowler, Thermal modeling and validation of temperature distributions in a prismatic lithium-ion battery at different discharge rates and varying boundary conditions, *Appl. Therm. Eng.* 96 (2016) 190–199.
- [37] Panchal, S., M. Rashid, F. Long, M. Mathew, M., Fraser, R. and Fowler, M., Degradation Testing and Modeling of 200Ah LiFePO₄ Battery for EV". SAE Technical Paper, 2018-01-0441.
- [38] M.N. Muratori, M. Canova, Y. Guezennec, A model order reduction method for the temperature estimation in a cylindrical li-ion battery cell, *Proc. ASME Dyn. Syst. Control Conf. 1* 2010, pp. 633–640.
- [39] D.R. Pendegast, E.P. DeMauro, M. Fletcher, E. Stimson, J.C. Mollendorf, A rechargeable lithium-ion battery module for underwater use, *J. Power Source.* 196 (2) (2011) 793–800.
- [40] C. Park and A.K. Jaura, Dynamic thermal model of li-ion battery for predictive behavior in hybrid and fuel cell vehicles, in SAE 2003- 01-2286, 2003.
- [41] M.A. Roscher, D.U. Sauer, Dynamic electric behavior and open-circuit-voltage modeling of LiFePO₄-based lithium ion secondary batteries, *J. Power Source.* 196 (2011) 331–336.
- [42] P. Ioannou, J. Sun, Robust Adaptive Control, Prentice Hall, 1996.
- [43] X. Lin, H. Fu, H.E. Perez, J.B. Siegel, A.G. Stefanopoulou, Y. Ding, M.P. Castanier, Parameterization and observability analysis of scalable battery clusters for onboard thermal management, *Oil Gas Sci. Technol.* vol.68, (2013) 165–178.
- [44] H. Maleki, J.R. Selman, R.B. Dinwiddie, H. Wang, High thermal conductivity negative electrode material for lithium-ion batteries, *J. Power Source.* 94 (1) (2001) 26–35.
- [45] W.H. McAdams, Heat Transmission, 3rd ed., McGraw-Hill, New York, NY, 1954.
- [46] G.M. Cavalheiro, T. Iriyama, G.J. Nelson, S. Huang, G. Zhang, Distribution on degradation of lithium-ion batteries, *J. Electrochem. En. Conv. Stor.* 17 (2) (2020) 1–8.